Grid independence behaviour of fluidized bed reactor simulations using the Two Fluid Model: Detailed parametric study

Schalk Cloete[1], Stein Tore Johansen[2] & Shahriar Amini[2]*

[1] NTNU Department of Energy and Process technology, Trondheim, NORWAY

[2] SINTEF Materials and Chemistry, Trondheim, NORWAY

*Corresponding author:

Dr. Shahriar Amini

Department of Process Technology

SINTEF Materials and Chemistry

Richard Birkelands Vei 3

7034 Trondheim, Norway

Phone: +47 46639721

Email: shahriar.amini@sintef.no

1   Abstract

This short communication builds on previous work on the grid independence behaviour of the Two Fluid Model in reactive bubbling fluidized bed simulations. Regarding hydrodynamic grid independence behaviour (the numerical accuracy with which phase segregation was resolved), the particle relaxation time was confirmed as being directly proportional to the cell size achieving sufficiently grid independent behaviour. This relationship held over different particle sizes, particle densities, gas densities, gas viscosities and drag laws, but the slope of the proportionality changed for particle relaxation times above 0.4. For reactive grid independence behaviour (the numerical accuracy with which reactor performance was resolved), the relationship between the particle relaxation time and the sufficiently grid independent cell size was more complex, depending not only on the resolution of phase segregation, but also on the kinetic rate implemented and on the permeability of the emulsion phase. Simple and practical rules of thumb were proposed for estimating the sufficiently grid independent cell size for hydrodynamic and reactive simulations. For most practical purposes, the simpler and more accurate hydrodynamic grid independent cell size correlation can safely be used to run sufficiently accurate bubbling fluidized bed reactor simulations.

2   Introduction

Grid independence behaviour of fluidized bed simulations carried out using the two fluid model (TFM) closed by the kinetic theory of granular flows (KTGF) remains a very important research topic even today, three decades after this approach was first proposed [1-3]. Firstly, TFM-KTGF simulations are used to derive industrial scale filtered models (e.g. [4-6]) which are enjoying significant research attention at present. Secondly, as shown in the first part of this work [7], larger particle sizes have much less stringent grid size requirements than smaller particle sizes and industrial sized beds using large particles (~500 μm) can already be simulated with current computational capacities.

These important applications of resolved TFM simulations require tedious and time consuming grid independence studies to be completed for every set of operating conditions simulated. Often, when a parametric CFD study is carried out, only one grid independence study is completed on the assumption that these guidelines can be used over the entire parameter space. This assumption is often invalid, however, implying that varying degrees of numerical error could be confounding the results obtained over the parameter space.

The first part of this work showed that grid independence behaviour scaled very well with the particle relaxation time. This correlation could be used to significantly shorten the grid independence work that must be done before each resolved TFM simulation campaign, but was only evaluated for

simulations carried out with different particle sizes. This second part of the work is therefore completed to assess this correlation by varying a broader range of simulation parameters that have a direct influence on the particle relaxation time.

3 Nomenclature

Main Symbol definitions:

α Volume fraction

Δ Sufficiently grid independent cell size (m)

ε Void fraction

ρ Density (kg/m³)

a Accleration (m/s²)

Ar Archimedes number $\left(\dfrac{g d_s^3 \rho_g \left(\rho_s - \rho_g \right)}{\mu_g^2} \right)$

c_3 Proportionality constant (s)

c_4 Proportionality constant (m)

d Particle diameter (m)

g Gravitational acceleration (m/s²)

k Reaction rate constant (s⁻¹)

m Mass (kg)

R^H Heterogeneous reaction rate (mol/(m³s))

Y Mass fraction

Sub- and superscript definitions:

$emul$ Emulsion

g Gas

hydro Hydrodynamic

react Reactive

s   Solids

4   Simulations

The simulation setup and data processing strategy followed in this short communication is identical to that reported in the first part of this work [7] except for the reaction kinetic description outlined in Section 4.1 below.

4.1   Reaction kinetics

A simple, catalytic conversion of five different gas species A, B, C, D and E to gas species A*, B*, C*, D* and E* respectively was simulated to occur on the surface of microscopic solid grains (*S*) within the particles used in the fluidized bed:

$$A + S \rightarrow A* + S$$
$$B + S \rightarrow B* + S$$
$$C + S \rightarrow C* + S$$
$$D + S \rightarrow D* + S$$
$$E + S \rightarrow E* + S$$
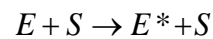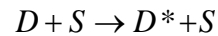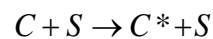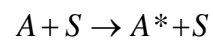
Mass transfer limitations were neglected on the assumption that mass transfer is much faster than the reaction rate on the surface of the grains. The validity of this assumption was confirmed in a previous publication by the authors [8].

The physical and chemical properties of all species were specified to be identical so that the reactions would not influence the hydrodynamics resulting in a non-linear interaction. This will significantly simplify the interpretation of results, enabling clearly decoupled conclusions regarding hydrodynamic and reaction kinetic grid independence to be drawn from each simulation.

The five reactions included in the system were set to run at different rates so that the influence of reaction rate on grid independence behaviour could be determined.

$$R_A^H = 20\alpha_s\rho_g \frac{Y_A}{Y_A + Y_{A*}}$$

$$R_B^H = 40\alpha_s\rho_g \frac{Y_B}{Y_B + Y_{B*}}$$

$$R_C^H = 80\alpha_s\rho_g \frac{Y_C}{Y_C + Y_{C*}}$$

Equation 1

$$R_D^H = 160\alpha_s\rho_g \frac{Y_D}{Y_D + Y_{D*}}$$

$$R_E^H = 320\alpha_s\rho_g \frac{Y_E}{Y_E + Y_{E*}}$$

The reaction rates in each cell (molar rate of change from species A to A*, B to B* etc. per unit volume) were then implemented as a source term into the species conservation equation. Since the species had identical properties and the reaction occurred in a 1:1 stoichiometric ratio, no mass or momentum source terms were required.

5 Results and discussion

Results will be presented in two main sections: an analysis of the hydrodynamic grid independence behaviour of the model and a similar analysis of the reactive grid independence. Nine new cases were simulated (Table 1), each over at least 5 different cell sizes.

Table 1: Fluidization velocity and material properties for the different cases considered in this study.

Case	Particle size (μm)	Particle density (kg/m³)	Gas density (kg/m³)	Gas viscosity (kg/(m.s))	Fluidization velocity (m/s)
1	200	2500	1.2	2.50E-5	0.273
2	400	2500	1.2	2.50E-5	0.523
3	800	2500	1.2	2.50E-5	1.080
4	400	1250	1.2	2.50E-5	0.322
5	400	5000	1.2	2.50E-5	0.844
6	400	2500	0.3	2.50E-5	0.777
7	400	2500	4.8	2.50E-5	0.340
8	400	2500	1.2	1.25E-5	0.687
9	400	2500	1.2	5.00E-5	0.389

5.1　Hydrodynamic grid independence

The hydrodynamic grid independence was quantified according to the phase segregation performance measure (the volume average of the RMS of the solids volume fraction over the bed region as described in [7]). Since the formation of structures (clusters and bubbles) is the primary factor influencing all transport phenomena occurring inside fluidized bed reactors, it is very important that the grid is sufficiently fine to capture these structures with at least reasonable accuracy. The phase segregation performance measure is a good indicator of the degree of structure resolution.

Following the same methodology as that outlined in the first part of this work [7], the particle relaxation time for each of the cases in Table 1 was calculated at different solids volume fractions. In this case, the particle relaxation time at a solids volume fraction of 0.02 produced a good fit as illustrated in Figure 1, although it should be stated that the fit remains good in the volume fraction range of $0 - 0.05$ ($R^2 > 0.98$). As discussed in [7], the solids volume fraction at which the particle relaxation time is calculated has a significant influence on the quality of the fit achieved and, in this case, the quality of the fit increasingly deteriorated above a solids volume fraction of 0.05. In this case, the solids volume fraction range of $0 - 0.05$ makes physical sense because it is the typical volume fraction experienced by freely moving particles inside the bubble. These particles will join into the surrounding solids structure if sufficient streamline curvature is resolved so that the particles' inertia cause deviations from the carrier phase streamlines [7].
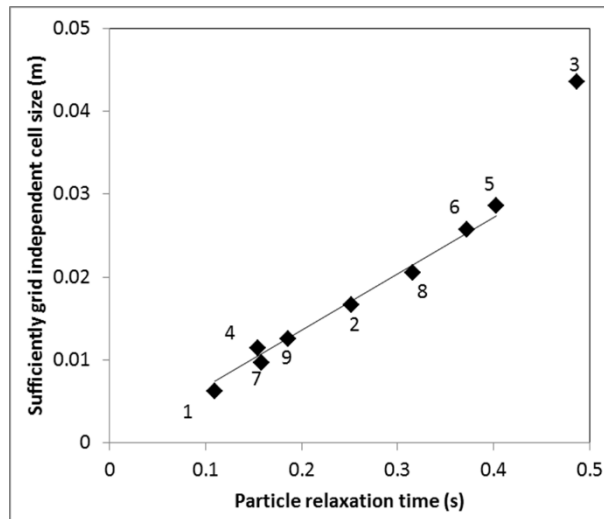

Figure 1: Correlation between the cell size achieving sufficient hydrodynamic grid independence and the particle relaxation time. The data points are numbered according to Table 1.

It is clear that the correlation holds very well for all cases except for case 3 (the largest particle size) where the grid independent cell size is predicted to be smaller than that shown by the actual simulation. When also adding the five cases completed in the first part of this work [7], it is shown that

case 3 is not an anomaly, but rather an indicator of a changing trend. The previous study investigated five particle sizes (200, 400, 600, 800 and 1000 μm) with a particle density of 2500 kg/m³, a gas density of 0.3 kg/m³ and a gas viscosity of 4.5E-5 kg/(m.s). The larger particle sizes in this previous study resulted in higher particle relaxation times than those shown in Figure 1.
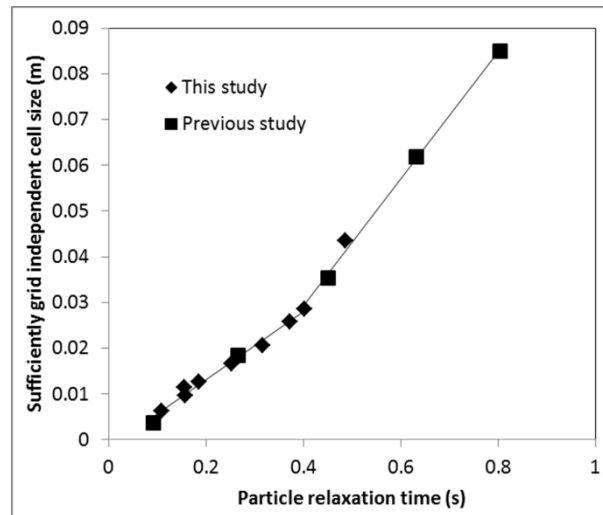

Figure 2: Correlation between the cell size achieving sufficient hydrodynamic grid independence and the particle relaxation time for all the data from this study and the previous study [7]. Two different linear trends are indicated.

The clear shift in the proportionality between the sufficiently grid independent cell size and the particle relaxation time around a relaxation time of 0.4 s is evident from Figure 2. In the first part of this work [7], this step change was not observed because of an insufficient number of data points (5 cases) and a single proportionality using the particle relaxation time at a solids volume fraction of 0.3 was established. The larger dataset available in this study (14 cases) clearly shows that this was not the complete picture and that the particle relaxation time at a volume fraction of 0.02 (typical volume fraction experienced by freely moving particles inside the bubbles) results in an excellent fit, provided that the step change in the proportionality can be explained.

The step change in proportionality suggests a change in the nature of the fluidization behaviour such as the change from Geldart B fluidization to Geldart D fluidization when $\left(\rho_s - \rho_g \right) d \geq 10^6$ [9] or $Ar \geq 176900$ [10]. To test the validity of this type of classification, the data in Figure 2 was plotted in Figure 3 where a distinction is made between Geldart B and Geldart D particles according to the original classification [9]. It is clear that this classification aligns well with the trend change. When using the Archimedes number criterion, however, all cases qualify as Geldart B.
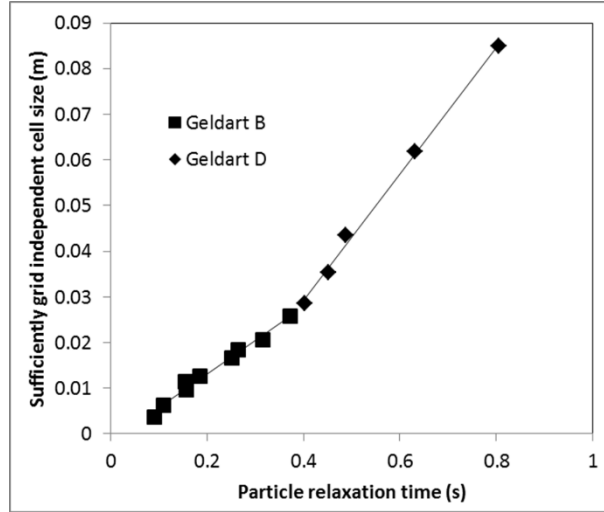
Figure 3: Correlation between the cell size achieving sufficient hydrodynamic grid independence and the particle relaxation time for all the data from this study and the previous study [7]. Particles are classified according to the classic Geldart groups [9].

The principle difference between Geldart B and Geldart D fluidization is that the interstitial gas rises slower than the most bubbles for Geldart B powders, but faster than most bubbles in Geldart D powders [11-13]. This transition significantly alters bubble dynamics and therefore offers one possible explanation for the trend change in Figure 3. However, the Archimedes number criterion should be more generically applicable as it can be extended to conditions other than air fluidization at standard temperature and pressure. Further exploration using correlations for minimum fluidization velocity [14], bubble size [15] and bubble rise velocity [16] reveal that the Geldart D criterion (interstitial gas rising faster than the bubbles) can be fulfilled in the bottom part of the bed in cases to the right of the trend change in Figure 3. The Geldart D criterion is not fulfilled for the majority of the domain, however, thus suggesting that changes in the bubble dynamics cannot fully explain the observed trend change.

Therefore, even though the fit in Figure 3 is very good, uncertainty exists surrounding the mechanism responsible for the trend change around a particle relaxation time of 0.4 s. Regardless of this uncertainty, a general rule of thumb for hydrodynamic grid independence can be proposed in Equation 2 where the subscript *sp* denotes a single particle.

$$\Delta_{hydro} \approx c_1 \tau \approx c_2 \tau_{sp} \approx c_3 u_{slip,sp} \qquad \text{Equation 2}$$

Equation 2 assumes that the single particle settling velocity is approximately proportional to the single particle relaxation time. This is valid as long as the difference between gas and solid densities is large as illustrated via the simple force balance on a settling particle below:

8

$$ma = drag + bouyancy$$

$$0 = \frac{mu_{slip}}{\tau} + \left(\rho_s - \rho_g\right)Vg$$

$$u_{slip} = -\frac{\left(\rho_s - \rho_g\right)Vg}{m}\tau \qquad\qquad \text{Equation 3}$$

$$= -\frac{\left(\rho_s - \rho_g\right)g}{\rho_s}\tau$$

$$\approx g\tau \text{ if } \rho_s >> \rho_g$$

The relaxation time can be somewhat cumbersome to calculate based on a given drag correlation, but the settling velocity of a single particle can be found from Heywood tables using a convenient online calculator [17]. Over the wide range of simulation cases investigated, the particle settling velocity from the Heywood tables is proportional to the particle relaxation time based on the selected drag law [3] with R^2=0.999.
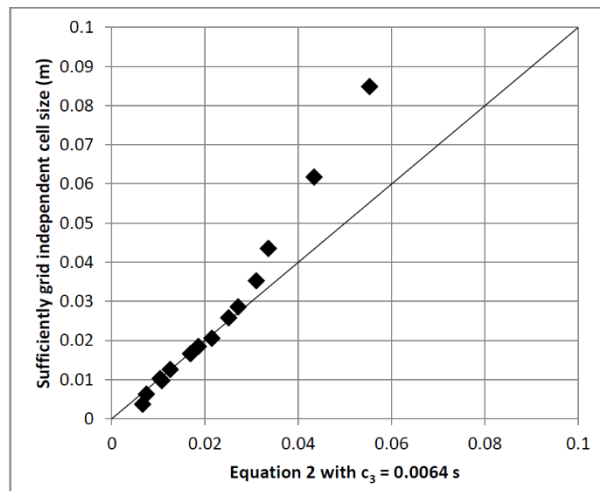

Figure 4: Illustration of a general rule of thumb for the sufficiently grid independent cell size (10% change upon cell halving) as

$$0.0064u_{slip,sp}.$$

The accuracy of the grid independence guideline proposed in Equation 2 is shown in Figure 4 where $c_3 = 0.0064$ s. It is shown that the proposed grid independence guideline will under-estimate the required cell size for large single particle settling velocities. However, the cell sizes at which this under-estimation becomes significant (> 3 cm) are already sufficiently large that a more conservatively small cell size can be afforded. The proposed simple guideline can therefore be used as a convenient generic rule of thumb for hydrodynamic grid independence in bubbling fluidized bed simulations carried out for different particles, gasses, temperatures and pressures.

Finally, this section will investigate whether the good correlation between the sufficiently grid independent cell size and the particle relaxation time achieved in Figure 2 also holds for a different drag law. The classical drag law of Wen and Yu [18] was selected and simulations were rerun for cases 2, 4, 6 and 8 in Table 1. The particle relaxation time for the Wen and Yu drag law was defined as follows:

$$\tau_s = \frac{\tau_{s_s}}{f}$$
Equation 4

$$\tau_{s_s} = \frac{\rho_s d_s^2}{18\mu_g}$$
Equation 5

$$f = \left(1 + 0.15\left(\alpha_g \operatorname{Re}_p\right)^{0.687}\right)\alpha^{-2.65}$$
Equation 6

The four new cases conducted with the Wen and Yu drag law are added to Figure 2 in Figure 5. It is clear that the relationship holds also for this alternative drag law.
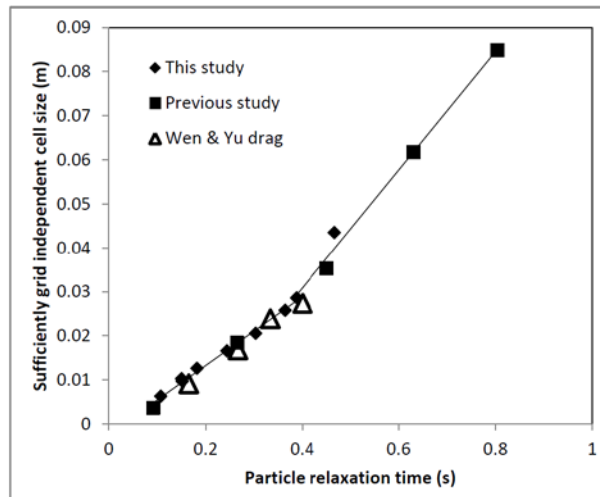

Figure 5: Correlation between the cell size achieving sufficient hydrodynamic grid independence and the particle relaxation time for all the data from this study and the previous study [7] carried out with the Syamlal and O'Brien drag law [3] as well as four new cases carried out with the Wen and Yu drag law [18].

5.2   Reactive grid independence

As discussed in the first part of this work [7], the reactive grid independence is judged based on the overall reactor performance (degree of gas conversion achieved). This study also investigated the effect of reaction kinetics by collecting data for five different kinetic rates from each simulation. A typical result from these five kinetic rates (Equation 1) is shown in Figure 6.

It is clear that a strong bubble-to-emulsion mass transfer resistance is present for all the kinetic rates. Even for the slowest rate (reactant A), most of the reactant remains in the solids-lean bubbles and

most solids are not in contact with any reactant. It is clear, however, that this mass transfer resistance becomes much more dominant as the kinetic rate is increased from left to right in Figure 6. At the highest reaction rate (reactant E), virtually no reactant is in contact with the dense emulsion phase.
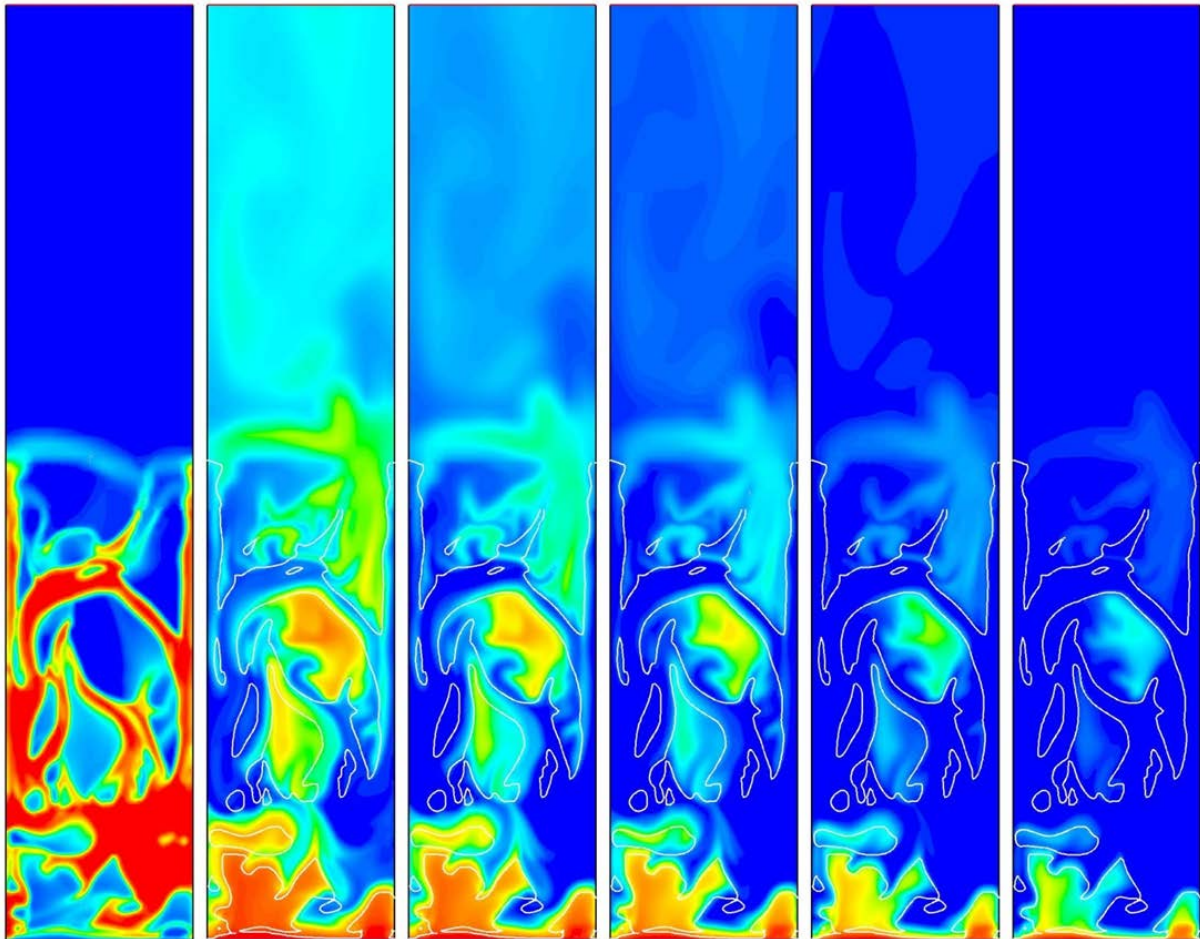

Figure 6: Instantaneous contours from case 2 in Table 1 solved on a fine mesh with 80 width-wise grid points. The left-most figure indicates the solids volume fraction. The remaining five figures represent (from left to right) the species mole fraction of reactants A, B, C, D and E as implemented in Equation 1. The bubble interface (the iso-surface where the solids volume fraction is 0.3) is also indicated in order to better visualize the bubble-to-emulsion mass transfer resistance.

This increasing importance of the bubble-to-emulsion mass transfer in determining the overall reactor performance is expected to have a significant effect on the reactive grid independence behaviour. The overall reaction rate is influenced both by the reaction kinetic and the mass transfer resistances, but only the mass transfer resistance is influenced by the grid spacing used in the simulation. Therefore, if the mass transfer resistance increases in significance (when the reaction kinetic resistance decreases in the case of fast kinetics), the overall reactor performance will become more sensitive to the cell size.

However, the reactive grid independence behaviour discussed in this section is expected to be more complex than the hydrodynamic grid independence behaviour discussed in the previous section. Naturally, the hydrodynamic grid independence (the degree of phase segregation resolved) will have a large effect on overall reactor performance. After all, if no phase segregation is resolved, there can be no mass transfer resistance. However, the importance of the bubble-to-emulsion mass transfer resistance will not only be influenced by the kinetic rate as discussed above, but also by the permeability of the emulsion phase. If small particles are used and the permeability of the emulsion phase becomes very low, bubble-to-emulsion mass transfer resistance will increase and so will the importance of accurate resolution of the gas-solids interface (where the majority of the reaction will now take place.

The combined effect of kinetic rate and emulsion phase permeability can be expressed as a ratio of the kinetic rate constant (s^{-1}) and the superficial slip velocity in the emulsion phase (m/s). Here, the assumption is made that convective mass transfer outweighs diffusive mass transfer which is a reasonable assumption given Péclet numbers based on the cell size in the order of 10. The aforementioned ratio has dimensions of m^{-1} and therefore is an indicator of the spatial reactant gradient that needs to be resolved to accurately describe the mass transfer.

It can be intuitively understood that higher reaction rates and lower emulsion permeabilities (causing low slip velocities in the emulsion phase) would require smaller cells to capture the large species gradients forming close to the bubble/cluster interface. Using the inverse of this indicator of the species gradient in combination with the cell size required for hydrodynamic grid independence (Equation 2), the data available in this study (5 kinetic rates for 9 cases) can be fitted according to Equation 7.

$$\Delta_{react} \approx c_3 u_{slip,sp} \left(\frac{\varepsilon_{emul} u_{slip,emul}}{c_4 k_{emul}} \right)^{0.6} \qquad \text{Equation 7}$$

In practice, applying Equation 7 to find the grid independent cell size can be cumbersome due to the need to calculate the slip velocity in the emulsion phase from the selected drag law. For this reason, a correlation for the minimum fluidization velocity [14] can be used to estimate the slip velocity in the emulsion phase as shown in Equation 8. Equation 8 correlates reasonably (R^2 = 0.935) with the slip velocity in the emulsion phase calculated from the drag law used in this study [3].

$$\varepsilon_{emul} u_{slip,emul} \approx U_{mf} \approx \frac{\left(\sqrt{27.2^2 + 0.0408 Ar} - 27.2 \right) \mu_g}{d_s \rho_s} \qquad \text{Equation 8}$$

The resulting fit is shown in Figure 7 where it is clear that Equation 7 and Equation 8 offer a reliable guideline for reactive grid independence over the wide range of particle sizes, particle densities, gas densities, gas viscosities and kinetic rates investigated in this study.
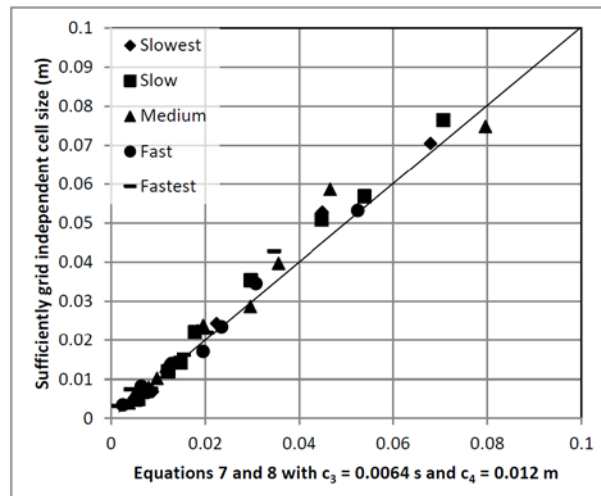

Figure 7: Illustration of a general rule of thumb for the sufficiently grid independent cell size (10% change upon cell halving) in reactive flows using Equation 7 and Equation 8 with $c_3 = 0.0064$ s and $c_4 = 0.012$ m..

The proposed rule of thumb for reactive grid independence (Equation 7) is more complex than the one for hydrodynamic grid independence (Equation 2) and also results in a somewhat poorer fit. It is therefore less practical and potentially also less reliable, implying that the rule of thumb for hydrodynamic grid independence will be the preferred option.

Using the hydrodynamic grid independence criterion would be merited if the hydrodynamic grid independent cell size was smaller than the reactive grid independent cell size. For the cases investigated in this study, this was generally the case for the slower reaction rates. Only the fastest reaction rates required smaller cells for reactive grid independence than for hydrodynamic grid independence. However, actual reactor performance data shows that the fast and fastest kinetics generally achieves reactor performance greater than 99.9%. From a practical point of view, this is essentially complete conversion, implying that reactive grid independence is not important in these cases. For the medium, slow and slowest reaction kinetics, on the other hand, the reactor converted between 80% and 99% of the incoming reactant, implying that accurate prediction of the reactor performance is important. Reactive grid independence will be achieved for these cases if hydrodynamic grid independence is ensured.

6 Summary and conclusions

The hydrodynamic and reactive grid independence behaviour of the TFM approach applied to bubbling fluidization was further investigated in this study. In particular, the merits of using the particle relaxation time to determine the grid independent cell size were investigated by conducting simulations over a range of particle sizes, particle densities, gas densities and gas viscosities.

Hydrodynamically, a clear proportionality between the grid independent cell size and the particle relaxation time was observed and confirmed for a different drag law. A moderate step change in this proportionality was observed at larger particle relaxation times (> 0.4 s). This step change was postulated to be related to the transition between Geldart B and Geldart D type fluidization in the lower regions of the bed. A simple and practical rule of thumb was proposed for estimating hydrodynamic grid independence in bubbling beds as $\Delta_{hydro} \approx c_3 u_{slip,sp}$. Setting $c_3 = 0.0064$ s will result in a situation where a halving of the cell size from $\sqrt{2}\Delta_{hydro}$ m to $\Delta_{hydro}/\sqrt{2}$ m will change the degree of phase segregation resolved by 10%.

In order to evaluate reactive grid independence behaviour, five different kinetic rates were tested. The cell size necessary to achieve satisfactory reactive grid independence increased with a decrease in the kinetic rate as the increased kinetic resistance reduced the importance of the bubble-to-emulsion mass transfer resistance. A rule of thumb for reactive grid independence was proposed as $\Delta_{react} \approx c_3 u_{slip,sp} \left(\varepsilon_{emul} u_{slip,emul} / c_4 k_{emul} \right)^{0.6}$. The reactive grid independent cell size depended not only on the degree of structure resolution, but also on the reactant species gradient expressed as the ratio of the reaction rate constant to the superficial gas slip velocity in the emulsion phase.

The proposed rule of thumb for the reactive grid independent cell size was more complex than the hydrodynamic cell size and may also be less reliable. However, for all cases where accurate prediction of the reactor performance was important, hydrodynamic grid independence was achieved on smaller cell sizes than reactive grid independence, implying that the cell size achieving sufficient grid independence with regard to reactor hydrodynamics can be used.

7 Acknowledgements

8 References

1. Gidaspow, D., R. Bezburuah, and J. Ding, *Hydrodynamics of Circulating Fluidized Beds, Kinetic Theory Approach*, in *7th Engineering Foundation Conference on Fluidization* 1992. p. 75-82.

2. Lun, C.K.K., et al., *Kinetic Theories for Granular Flow: Inelastic Particles in Couette Flow and Slightly Inelastic Particles in a General Flow Field.* Journal of Fluid Mechanics, 1984. **140**: p. 223-256.

3. Syamlal, M., W. Rogers, and T.J. O'Brien, *MFIX Documentation: Volume 1, Theory Guide.* 1993, Springfield: National Technical Information Service.

4. Wang, W. and J. Li, *Simulation of gas-solid two-phase flow by a multi-scale CFD approach-of the EMMS model to the sub-grid level.* Chemical Engineering Science, 2007. **62**(1-2): p. 208-231.

5. Wang, J., W. Ge, and J. Li, *Eulerian simulation of heterogeneous gas-solid flows in CFB risers: EMMS-based sub-grid scale model with a revised cluster description.* Chemical Engineering Science, 2008. **63**(6): p. 1553-1571.

6. Andrews, A.T., P.N. Loezos, and S. Sundaresan, *Coarse-grid simulation of gas-particle flows in vertical risers.* Industrial and Engineering Chemistry Research, 2005. **44**(16): p. 6022-6037.

7. Cloete, S., S.T. Johansen, and S. Amini, *Grid independence behaviour of fluidized bed reactor simulations using the Two Fluid Model: Effect of particle size.* Powder Technology, 2015. **269**(0): p. 153-165.

8. Cloete, S., S.T. Johansen, and S. Amini, *An assessment of the ability of computational fluid dynamic models to predict reactive gas–solid flows in a fluidized bed.* Powder Technology, 2012. **215-216**(0): p. 15-25.

9. Geldart, D., *Types of gas fluidization.* Powder Technology, 1973. **7**(5): p. 285-292.

10. Goossens, W.R.A., *Classification of fluidized particles by Archimedes number.* Powder Technology, 1998. **98**(1): p. 48-53.

11. Yang, W.-C., *Handbook of Fluidization and Particle-Fluid Systems: Chapter 3*. 2003: Marcel Dekker.

12. Kunii, D. and O. Levenspiel, *Fluidizaton Engineering: Chapter 4*. 2nd ed. 1991: Butterworth-Heinemann.

13. Davidson, J.F., R. Cllift, and D. Harrison, *Fluidization: Chapter 1*. 2nd ed. 1985: Academic Press Inc.

14. Bi, H.T. and J.R. Grace, *Flow regime diagrams for gas-solid fluidization and upward transport.* International Journal of Multiphase Flow, 1995. **21**(6): p. 1229-1236.

15. Cai, P., et al., *Quantitative estimation of bubble size in PFBC.* Powder Technology, 1994. **80**(2): p. 99-109.

16. Davidson, J.F., Harrison, D., ed. *Fluidized particles*. Cambridge University Press:Chapter 6. 1963: New York.

17. *Filtration & Separation.com*. Available from: http://www.filtration-and-separation.com/settling/settling.htm.

18. Wen, C.Y. and Y.H. Yu, *Mechanics of Fluidization.* Chemical Engineering Progress Symposium Series, 1966. **62**: p. 100-111.